

# Electrophysiological studies of transgenic long QT type 1 and type 2 rabbits reveal genotype-specific differences in ventricular refractoriness and His conduction

Katja E. Odening,<sup>1,2\*</sup> Malcolm Kirk,<sup>1\*</sup> Michael Brunner,<sup>1,2\*</sup> Ohad Ziv,<sup>1\*</sup> Peem Lorvidhaya,<sup>1</sup> Gong Xin Liu,<sup>1</sup> Lorraine Schofield,<sup>1</sup> Leonard Chaves,<sup>1</sup> Xuwen Peng,<sup>3</sup> Manfred Zehender,<sup>2</sup> Bum-Rak Choi,<sup>1</sup> and Gideon Koren<sup>1</sup>

<sup>1</sup>Cardiovascular Research Center, Division of Cardiology, Rhode Island Hospital, Warren Alpert Medical School of Brown University, Providence, Rhode Island; <sup>2</sup>Innere Medizin III, Kardiologie, University Hospital Freiburg, Freiburg, Germany; and <sup>3</sup>Department of Comparative Medicine, Pennsylvania State University College of Medicine, Hershey, Pennsylvania

**Odening KE, Kirk M, Brunner M, Ziv O, Lorvidhaya P, Liu GX, Schofield L, Chaves L, Peng X, Zehender M, Choi B, Koren G.** Electrophysiological studies of transgenic long QT type 1 and type 2 rabbits reveal genotype-specific differences in ventricular refractoriness and His conduction. *Am J Physiol Heart Circ Physiol* 299: H643–H655, 2010. First published June 25, 2010; doi:10.1152/ajpheart.00074.2010.—We have generated transgenic rabbits lacking cardiac slow delayed-rectifier K<sup>+</sup> current [ $I_{Ks}$ ; long QT syndrome type 1 (LQT1)] or rapidly activating delayed-rectifier K<sup>+</sup> current [ $I_{Kr}$ ; long QT syndrome type 2 (LQT2)]. Rabbits with either genotype have prolonged action potential duration and QT intervals; however, only LQT2 rabbits develop atrioventricular (AV) blocks and polymorphic ventricular tachycardia. We therefore sought to characterize the genotype-specific differences in AV conduction and ventricular refractoriness in LQT1 and LQT2 rabbits. We carried out in vivo electrophysiological studies in LQT1, LQT2, and littermate control (LMC) rabbits at baseline, during isoproterenol infusion, and after a bolus of dofetilide and ex vivo optical mapping studies of the AV node/His-region at baseline and during dofetilide perfusion. Under isoflurane anesthesia, LQT2 rabbits developed infra-His blocks, decremental His conduction, and prolongation of the Wenckebach cycle length. In LQT1 rabbits, dofetilide altered the His morphology and slowed His conduction, resulting in intra-His block, and additionally prolonged the ventricular refractoriness, leading to pseudo-AV block. The ventricular effective refractory period (VERP) in right ventricular apex and base was significantly longer in LQT2 than LQT1 ( $P < 0.05$ ) or LMC ( $P < 0.01$ ), with a greater VERP dispersion in LQT2 than LQT1 rabbits. Isoproterenol reduced the VERP dispersion in LQT2 rabbits by shortening the VERP in the base more than in the apex but had no effect on VERP in LQT1. EPS and optical mapping experiments demonstrated genotype-specific differences in AV conduction and ventricular refractoriness. The occurrence of infra-His blocks in LQT2 rabbits under isoflurane and intra-His block in LQT1 rabbits after dofetilide suggest differential regional sensitivities of the rabbit His-Purkinje system to drugs blocking  $I_{Kr}$  and  $I_{Ks}$ .

long QT syndrome; His-Purkinje conduction; rapidly activating delayed-rectifier potassium current; slow delayed-rectifier potassium current; transgenic rabbit model; pharmacogenomics; ventricular effective refractory period dispersion; in vivo electrophysiological study

THE INHERITED LONG-QT SYNDROME (LQTS) is a genetically heterogeneous arrhythmic disease characterized by impaired car-

diac repolarization leading to QT prolongation, polymorphic ventricular tachycardia (pVT), and sudden cardiac death (SCD) (reviewed in Ref. 34). The most common forms of LQTS, type 1 and type 2 (LQT1 and LQT2), account for >90% of the genotyped cases and are due to loss-of-function mutations in KvLQT1 [ $\alpha$ -subunit of slow delayed-rectifier K<sup>+</sup> current ( $I_{Ks}$ )] (11) or HERG [ $\alpha$ -subunit of rapidly activating delayed-rectifier K<sup>+</sup> current ( $I_{Kr}$ )] (9), respectively.

The known triggers for pVTs in LQTS vary from genotype to genotype. For example, in LQT1, physical exercise typically provokes pVTs, whereas, in LQT2, auditory stimuli and startle, e.g., a sudden sympathetic surge during episodes of rest, often cause the arrhythmias (reviewed in Ref. 34), suggesting different modes of arrhythmia initiation. Although numerous studies of single myocyte and computer modeling suggest that slow heart rate is a necessary condition for early afterdepolarization (EAD) generation that leads to pVTs (40), a limited number of literature describes conduction anomalies in the conduction system in patients with LQTS, let alone with differences in various LQT types. Atrioventricular (AV) conduction block due to markedly prolonged ventricular refractoriness, termed pseudo-AV block by Rosenbaum and Acunzo (35), has been described as the primary mechanism responsible for conduction abnormalities in patients with LQTS (14). However, a few case reports also described true infranodal AV block in these patients (16, 31). Despite the relatively infrequent overall occurrence of AV conduction abnormalities (30), they are clearly associated with a poorer prognosis. In neonates, AV block has been associated with an elevated risk of arrhythmia and is more frequent in patients with mutations in HERG, particularly within the pore region (18, 27). Similarly, in adults with LQT2, AV block is a proven trigger for arrhythmias, preceding the onset of pVT (36). However, the level of the AV block in patients with LQT2 remains undefined.

Patients with LQTS are rarely inducible for ventricular tachycardia or ventricular fibrillation (VT/VF) with standardized programmed ventricular stimulation, and VT inducibility lacks a predictive value (2, 5). Hence, invasive electrophysiological studies (EPS) are not part of the standard evaluation of patients with LQTS (34), and, consequently, genotypic differences in standard electrophysiological parameters have not been assessed. Moreover, the consequences of the loss of either  $I_{Kr}$  or  $I_{Ks}$  on His-Purkinje conduction have not been studied systematically, and our understanding of His-Purkinje conduction in different types of LQTS is very limited, although both  $I_{Kr}$  and  $I_{Ks}$  are known to be expressed in rabbit and canine Purkinje cells (8, 17).

\* K. E. Odening, M. Kirk, M. Brunner, and O. Ziv contributed equally to this work.

Address for reprint requests and other correspondence: G. Koren, Cardiovascular Research Center, Cardiology Division, Rhode Island Hospital, Providence, RI 02903 (e-mail: gideon\_koren@brown.edu).

In rabbits, unlike mice (3, 23), the cardiac action potential and electrocardiogram (ECG) are markedly similar to those of the human heart, and repolarization is determined by similar potassium currents (37, 39). We therefore reasoned that studying the impact of mutations of human ion channels in rabbits would provide important additional mechanistic insights into impaired cardiac repolarization and arrhythmogenesis in LQTS. To that end, we have generated transgenic rabbits overexpressing dominant-negative pore mutants of the human KvLQT1 (KvLQT1-Y315S, LQT1) or HERG (HERG-G628S, LQT2) in the heart (4). These rabbit models demonstrate prolonged QT intervals (in both LQT1 and LQT2 rabbits) and SCD due to pVT (in LQT2 rabbits) and have allowed us to investigate the mechanisms underlying SCD in LQTS (4, 42). Importantly, LQT2 rabbits developed AV conduction blocks, which occasionally were associated with pVT, spontaneously without anesthesia, as well as under anesthesia with  $I_{Ks}$ - and inward rectifier potassium current ( $I_{K1}$ )-blocking drugs (isoflurane and midazolam, respectively) (4, 29). By contrast, none of the LQT1 rabbits showed altered AV conduction.

To further investigate the mechanisms of AV block in LQT rabbits, we undertook the first detailed transvenous *in vivo* catheter-based EPS in rabbits, including His signal recordings supplemented by *ex vivo* optical mapping of the AV node/His region, and characterized the differential physiological effects of eliminating  $I_{Kr}$  or  $I_{Ks}$  on AV conduction and ventricular refractoriness.

## METHODS

All animal studies were performed in accordance with the local guidelines of the institutions and only after approval by the Institutional Animal Care and Use Committee in accordance with the *Guide for the Care and Use of Laboratory Animals* published by the U.S. National Institutes of Health (NIH Publication No. 85-23, revised 1996).

**Minimally invasive *in vivo* EPS.** The protocol was based on standard protocols used in humans, adapted to rabbit physiology. Male LQT1, LQT2, and littermate control (LMC) rabbits were anesthetized with intramuscular ketamine/xylazine (25 mg/kg and 3.75 mg/kg, respectively) and buprenorphine (0.03 mg/kg), intubated, and ventilated with isoflurane (1–2%, fraction of inspired  $O_2 = 0.5$ ). Blood pressure and peripheral oxygen saturation were measured continuously. Steerable 4-Fr decapolar and 4-Fr quadripolar EP catheters (Irvine Biomedical, Irvine, CA) were inserted in the right

femoral and right jugular veins through 4-Fr sheaths and placed in the right atrium and ventricle, guided by fluoroscopy and pacing thresholds (Fig. 1A). Signals from the His bundle were obtained with the ventricular EP catheter [right ventricle (RV) base] (Fig. 1B). During the procedure, 12-lead surface, two intra-atrial, and five intraventricular ECG signals were recorded continuously using the EP-Bard-System Software OS2/warp (kindly provided by Bard, Lowell, MA), filtered with a bandwidth of 30–250 Hz (intracardiac signals) and 0.01–100 Hz (surface ECG). Of note, most rabbits displayed an incomplete RBBB-like QRS pattern in V1 regardless of genotype (Fig. 1B), even before EP catheter placement, most likely because of the slightly different intrathoracic position of the rabbit's heart. EPS were performed at a stimulation cycle length (CL) of 240 ms. The following parameters were analyzed as previously described (3). AH (atrium to His) and HV (His to ventricle) intervals were measured. Antegrade and retrograde Wenckebach CL (AVWCL/VAWCL) were characterized as the longest CL resulting in Wenckebach block. Atrial effective refractory period (AERP), AV-nodal/His-Purkinje effective refractory period (AVN/His-ERP), and ventricular effective refractory periods (VERP) in RV apex (VERPapex) and septal RV base (VERPbase) position were analyzed by progressively shortening the S2 interval in 10-ms steps after 8-beat S1 trains. The VERP measurements were validated on initial studies using a step-up protocol with continuous ventricular S1 pacing trains and progressive lengthening of the S2 interval, starting below VERP, which was defined as the longest S2 that failed to capture the myocardium. VERP dispersion, defined as the absolute value of the difference in VERP between base and apex, was calculated. Programmed ventricular stimulation was performed with one, two, and three extra stimuli in apical and basal positions to examine VT/VF inducibility.

EPS were performed at baseline and during isoproterenol (ISO) infusion (0.10–0.25  $\mu\text{g}/\text{min}$  to increase the spontaneous heart rate to 120%). Following washout of ISO, the  $I_{Kr}$  blocker dofetilide (0.02  $\mu\text{g}/\text{kg}$ ) was given as a bolus intravenously (in a concentration similar to that described in Ref. 22). QT and RR intervals were measured immediately before and every 2 min after the dofetilide bolus for a monitoring period of 60 min.

**Choice of anesthetic drug.** The results of a previous study (29) on the effect of anesthetic drugs on QT intervals in LQT and LMC rabbits guided our choice of anesthetic agent. Briefly, isoflurane and the potential alternatives thiopental or propofol all affected QT duration, either by prolonging the QT index (QTi) in LQT2 and LMC, but not in LQT1 rabbits (isoflurane, thiopental), or by prolonging the QTi in all three genotypes (propofol) (29). Moreover, because of the poor analgesic effect of propofol and thiopental (12), they offered no advantages over isoflurane. The only drug that did not alter the QTi in any genotype was ketamine. Because the depth of anesthesia achieved by ketamine was insufficient for the long duration of the EPS, we

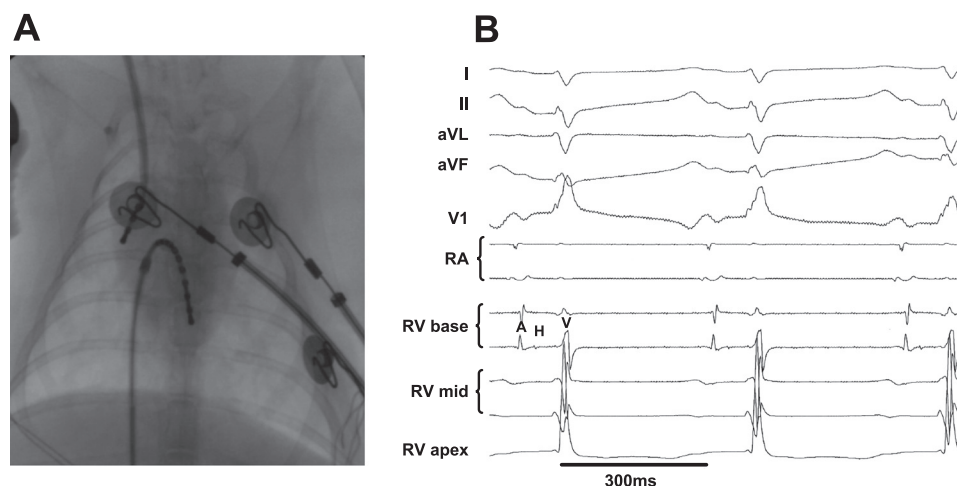


Fig. 1. A: fluoroscopic image showing catheter placement in right atrium (RA) and right ventricle (RV). B: surface electrocardiogram (ECG) (standard limb leads I, II, aVL, aVF, and chest lead V1) and intracardiac ECG recordings during normal sinus rhythm in male long QT syndrome type 2 (LQT2) rabbit. Note that His bundle electrogram is seen in RVbase electrodes. A, atrial signal; H, His signal; V, ventricular signal.

chase isoflurane. However, one should be aware that, because of its  $I_{Ks}$ -blocking properties, isoflurane creates a “drug-induced LQT1 phenotype” in LMC rabbits, reducing or abolishing potential differences in cardiac repolarization and AV conduction between LQT1 and LMC rabbits.

**Heart rate-corrected QT<sub>i</sub>.** To evaluate the effect of the  $I_{Kr}$ -blocker dofetilide (32) on QT duration, we applied the following previously established heart rate correction formulas for the expected QT interval under isoflurane anesthesia (4): LMC,  $QT_{\text{expected}} = 0.4 \times RR + 92$ ; LQT1,  $QT_{\text{exp}} = 0.42 \times RR + 74$ ; LQT2:  $QT_{\text{exp}} = 0.65 \times RR + 76$ . The QT<sub>i</sub> was defined as the percentage of the observed vs. the expected QT, a QT<sub>i</sub> >100% representing a drug-induced prolongation of QT.

**Electrophysiological patch-clamp recordings.** Isolation of myocytes by standard enzymatic techniques and patch-clamp recordings were performed as described previously (4). Apical ventricular myocytes were isolated from hearts of transgenic LQT and LMC rabbits (males, age 7–17 mo, 2.8–4.8 kg).  $I_{Ks}$  was recorded from a holding potential of  $-40$  mV to  $+30$  mV at the basal level and after ISO exposure (100 nM) in the presence of the  $I_{Kr}$ -blocker E4031 (5  $\mu$ M).  $I_{Ks}$  was defined as the current difference between the end pulse and the initial pulse. Chromanol 293B (50  $\mu$ M) was used to block  $I_{Ks}$  after ISO exposure.

**Optical mapping of AV-His-Purkinje conduction.** To further investigate the level of AV conduction block noted at EPS in LQT1 rabbits early after bolus administration of dofetilide, we performed optical mapping studies of perfused AV node (AVN) and His junctions of LQT1 ( $n = 5$ , age  $13.6 \pm 4.4$  mo,  $5.1 \pm 0.6$  kg, females), LMC ( $n = 3$ , age  $11.3 \pm 4.4$  mo,  $5.1 \pm 0.3$  kg, males), and LQT2 ( $n = 3$ , age  $9.7 \pm 3.8$  mo,  $4.4 \pm 0.3$  kg, males) rabbit hearts. LQT1 females were chosen because of a lack of males (used for other studies) and because we observed no gender differences in the response of LQT1 rabbits to drugs such as anesthetic agents (29) or dofetilide or in any electrophysiological parameters such as AVN conduction in vivo (Odening KE, Liu GX, Kirk M, Brunner M, Schofield L, Chaves L, Zehender M, Peng X, Koren G, unpublished observation). Heart preparation and retrograde perfusion were performed as described in detail previously (4). In brief, hearts were stained with a voltage-sensitive dye, di-4 ANEPPS (Invitrogen). Blebbistatin (5  $\mu$ M) was added to the perfusate to reduce motion artifacts (13). The triangle of Koch was exposed by removing the right atrial appendage and by bringing the incision across the lateral wall of the right atrium to the inferior vena cava, thus exposing the AVN and the His bundle.

The optical apparatus was described previously (6). Fluorescence images from the triangle of Koch were focused on a CMOS camera (100  $\times$  100 pixels, Ultima-L; Scimedica). The field of view was set to  $4 \times 4$  mm ( $40 \times 40$   $\mu$ m spatial resolution) to locate and record signals from the AV junction to obtain high-resolution His signal recordings and map His activation (using a 25-mm f0.95 Navitar video lens). As described (7, 19, 20), the fluorescence signal recorded from the single pixel at the AV junction is the sum of multiple cells in the region, including cells from deeper layers (depth of the field of view 200  $\mu$ m). At the proximal junction, a summation of atrial, AV nodal, and proximal His signals is seen, whereas at the distal AV junction, a summation of His and ventricular signals is seen. These summation signals, however, demonstrate multiple upstrokes, since the timing of the different tissue types in this region varies with time. To validate optical signal source in this region, we simultaneously recorded electrograms with a traditional bipolar electrode used in our in vivo studies (described above). We mapped the propagation of each upstroke and correlated optical signal upstrokes with timing of electrograms on bipolar recordings. The sampling rate of optical recordings was set to 1,000 frames/s, and data were analyzed with custom-built software using Interactive Data Language (ITT Visual Information Solutions, Boulder, CO). The signals were recorded during atrial pacing at 400 ms CL (to mimic heart rates seen in in vivo studies with anesthetized rabbits) at baseline and during dofetilide ( $10^{-9}$  mol/l)

infusion. Hearts were continuously perfused with a standard  $10^{-9}$  mol/l dofetilide infusion (as described in Refs. 25 and 33), and optical mapping recordings were started a minimum of 5 min after the initiation of the perfusion.

**Optical mapping data analysis.** The activation and repolarization time points at each site were determined from  $(dF/dt)_{\text{max}}$  and  $(d^2F/dt^2)_{\text{max}}$ , respectively (6). Data were filtered using a spatial Gaussian filter ( $3 \times 3$  pixel), and first/second derivatives ( $dF/dt$ ,  $d^2F/dt^2$ ) were calculated using a polynomial filter (3rd order, 13 points). The conduction velocity (CV) of the His bundle was calculated by manually isolating the His activation wavefront as follows: to avoid overlap with AV nodal conduction from His conduction in our CV calculation, we plotted the activation time along the line drawn from the AV junction toward the end of the His activation detected with our system. The activation time plot of the AV-His region shows two steps (see Fig. 6E): first, a rapid rise of activation time delay due to slow conduction in the AV node; and second, a slow rise of activation time delay due to rapid conduction in the His region. The latter region with shallow activation time was used to calculate a gradient of activation time from the linear regression slope. Because the optical mapping data of AV conduction is comprised of compact nodal, lower nodal bundle, and His conduction (20, 21), we reasoned that the location of the true proximal His bundle was where the rapid activation was stable, i.e., no acceleration at the distal (rightward) aspect of the activation map. We focused on this region in calculating His conduction velocity and in looking for the site of block. CVs may be underestimated, since the His bundle penetrates into the deeper layer of the septum, and the true His conduction axis cannot be easily focused on the focal plane of our optical system.

**Immunohistochemistry.** Heart tissue from the region corresponding to the optical mapping field of view was excised and fixed with neutral buffered formalin (10%), embedded into paraffin, and cut in 10- $\mu$ m serial sections. After deparaffinization and rehydration, the slides were incubated with anti-neurofilament 70 antibodies (1:1,500, mouse monoclonal, MAB 1615, Chemicon, as described in Ref. 20) and goat-anti-mouse horseradish peroxidase secondary antibody. Masson's Trichrome staining was used to identify the collagenous connective tissue.

**Statistical analysis.** For normally distributed values, we used Student's *t*-test (paired and unpaired) to compare the means of two groups and the Mann-Whitney test to compare values not normally distributed. We used Fisher's exact test for categorical variables. Analysis was performed with Prism 4 for Windows (Graphpad, San Diego, CA). All data are presented as means  $\pm$  SD unless described otherwise, and a *P* value  $\leq 0.05$  was considered significant.

## RESULTS

Successful EPS were performed in 11 LMC, 11 LQT1, and 9 LQT2 rabbits. Mean age (months) was  $28.9 \pm 2$  (LMC),  $25.7 \pm 6$  (LQT1), and  $16 \pm 11$  (LQT2) (*P* = not significant LMC vs. LQT1). LQT2 rabbits were significantly younger when studied (*P* < 0.05) because of their increased spontaneous mortality (4). The duration of the EP study procedure was  $219 \pm 85$  min; the duration of the entire procedure from initiation of anesthesia until completion of the final suture was  $429 \pm 85$  min, with no significant differences among groups. All animals included in this study survived the EPS. Of note, one LQT2 male died of pVT within 48 h after EPS.

**AV conduction: Spontaneous infra-His block in LQT2.** Baseline heart rates [RR intervals (ms): LMC,  $371 \pm 85$ ; LQT1,  $335 \pm 45$ ; LQT2,  $337 \pm 54$ ] and AERP did not differ among genotypes (Table 1), with no significant change over the duration of the baseline experiment. Although PR intervals were also similar in all three genotypes (Table 1), we found differences in His conduction, with a trend toward a longer HV duration in

Table 1. Surface ECG and intracardiac electrophysiologic parameters in LMC, transgenic LQT1, and LQT2 rabbits

	RR, ms	PQ, ms	QT, ms	AERP, ms	AH, ms	HV, ms	AV/His-WCL, ms	VAWCL, ms
LMC ( <i>n</i> = 11)	353.8 ± 20.7	86.2 ± 15.4	228.3 ± 11.0	113.3 ± 5.8	57.7 ± 4.4	27.7 ± 2.6	194.0 ± 11.7	170.0 ± 8.5
LQT1 ( <i>n</i> = 11)	335.2 ± 12.6	76.1 ± 8.2	208.5 ± 7.8	115 ± 9.2	51.0 ± 3.9	27.9 ± 1.6	165.8 ± 7.4 <sup>b</sup>	167.8 ± 8.5 <sup>a</sup>
LQT2 ( <i>n</i> = 9)	334.9 ± 20.2	82.7 ± 8.2	316.7 ± 20.3 <sup>d,e</sup>	116 ± 11.1	49.3 ± 3	31.1 ± 2.1	227.5 ± 16 <sup>c,e</sup>	203.8 ± 11.9 <sup>c,e</sup>

All values are presented as means ± SE; *n*, no. of experiments. LMC, littermate control; LQT1, long QT syndrome type 1; LQT2, long QT syndrome type 2; AERP, atrial effective refractory period; AH, atrium to His; HV, His to ventricle; AV, atrioventricular; WCL, Wenckebach cycle length; VAWCL, retrograde WCL. <sup>a</sup>*P* < 0.05 vs. LQT2. <sup>b</sup>*P* < 0.01 vs. LQT2. <sup>c</sup>*P* < 0.05 vs. LMC. <sup>d</sup>*P* < 0.01 v. LMC. <sup>e</sup>*P* < 0.01 vs. LQT1.

LQT2 than in LQT1 or LMC rabbits and significantly longer duration of antegrade AV- and retrograde VA-Wenckebach cycles (AV/His-WCL, VAWCL) in LQT2 than in LQT1 or LMC rabbits (Table 1). Moreover, intermittent, spontaneous second-degree AV block was detected in 6 of 9 LQT2 rabbits during isoflurane anesthesia (Fig. 2A) but not in LQT1 or LMC rabbits (Fig. 2, B and C).

To elucidate the level of the AV block, we investigated the possibility of ventricular pacing during the episodes of AV block, when the initiation of ventricular pacing was timed to the upstroke of the T wave at the same interval as the His signal would occur. We found that our first stimulus indeed captured the ventricle, proving that the ventricle was not refractory and hence that the AV block was above the ventricular level (Fig. 2D). His bundle recordings also revealed clear His signals at the time of block, suggesting that the AV block occurred at the infra-His level (Fig. 2A). During fast pacing (CL of 170 ms), we observed decremental HV conduction in LQT2 rabbits

before the infra-His block, further supporting the block being within the His-Purkinje system (Fig. 2E). During atrial stimulation with progressive shortening of the S2 interval, we again observed an AV block at the infra-His level, demonstrating a prolonged His-Purkinje-ERP in LQT2 rabbits (176.7 ± 15.8 ms) (Fig. 2F). In contrast, in five of seven LQT1 and four of six LMC rabbits, AV conduction persisted until the AERP was reached. In the remaining rabbits, in which AVNERP was reached before AERP, the AVNERP was shorter than in LQT2 rabbits [AVNERP (ms): LQT1, 115 ± 16.7, *P* < 0.05 vs. LQT2; LMC, 133 ± 14, *P* = 0.07 vs. LQT2].

We next determined the effects of ISO on AV conduction. ISO increased the heart rate similarly in all genotypes [RR intervals (ms): LMC, 286 ± 33; LQT1, 272 ± 38; LQT2, 293 ± 36] and abolished the genotype differences in AV/His-WCL [AV/His-WCL (ms): LMC, 160.0 ± 9.6; LQT1, 165.7 ± 6.5; LQT2, 171.7 ± 8.3] by significantly shortening the AV/His-WCL in LQT2 (*P* < 0.01) and LMC (*P* < 0.05). As expected, ISO did not affect

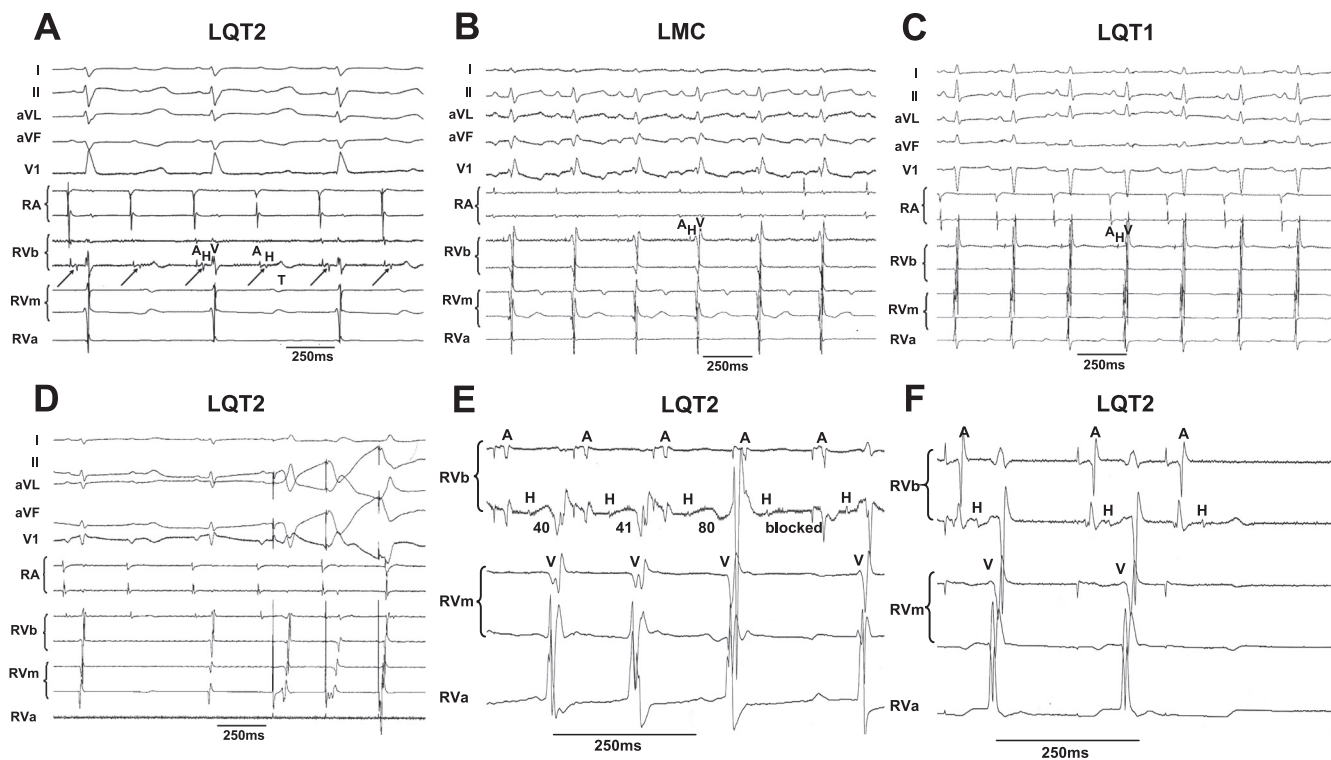


Fig. 2. A: representative tracing of LQT2 rabbit with atrioventricular (AV) conduction block under isoflurane anesthesia. The His bundle electrogram shows the infra-His level of the AV conduction block. T, T wave. B: representative ECG tracing in littermate control (LMC) under isoflurane: absence of AV block. C: representative ECG tracing of long QT syndrome type 1 (LQT1) under isoflurane: absence of AV block. D: ventricular pacing, and capture during AV 2:1 block, in the LQT2 rabbit shown in A indicates that the block is not due to ventricular refractoriness. E: decremental His conduction and infra-His Wenckebach at 170-ms stimulation cycle length (CL) in LQT2 rabbit. Indicated are durations of HV intervals. F: infra-His effective refractory period (ERP) in LQT2 rabbit at S1 of 240 ms and S2 of 190 ms. RVb, RV base; RVm, RV mid; RVa, RV apex.

AV/His-WCL in LQT1 rabbits. ISO abolished the spontaneous infra-His block in all LQT2 rabbits.

**VERP and VERP dispersion.** Both VERPapex and VERPbase were significantly longer in LQT2 than in LQT1 and LMC rabbits (Fig. 3A). In contrast, no differences in VERP were seen between LQT1 and LMC rabbits, although the QT intervals in free-moving LQT1 rabbits were also prolonged compared with LMC rabbits (4). In line with these findings, QT intervals were significantly longer in LQT2 than in LQT1 or LMC rabbits (Table 1), whereas the QT interval did not differ between LQT1 and LMC rabbits (similar to previous reports, e.g., see Ref. 29). We observed a nonsignificant trend toward a longer VERP in the RV base than in the apex in all three genotypes, with the most pronounced base-to-apex difference in VERP in LQT2 rabbits ( $P = 0.09$ , Fig. 3A). Eight of nine LQT2 rabbits had a longer VERPbase than VERPapex, whereas only five of eight LQT1 and six of nine LMC rabbits showed a longer VERPbase than VERPapex. The VERP dispersion (absolute value of the difference between base and apex) was significantly larger in LQT2 ( $P < 0.05$ , Fig. 3B) than in LQT1 or LMC rabbits.

We further investigated the response of ventricular refractoriness to ISO. ISO significantly shortened VERPapex and

VERPbase in LQT2 rabbits (Fig. 3A). However, this shortening was more pronounced in the base ( $\Delta\text{VERP}_{\text{basal-ISO}}$ :  $31 \pm 5.7$  ms) than in the apex ( $\Delta\text{VERP}_{\text{basal-ISO}}$ :  $18 \pm 5$  ms,  $P < 0.05$ ), hence, ISO tended to reduce the spatial VERP dispersion in LQT2 rabbits ( $P = 0.1$ , Fig. 3B). Moreover, since ISO did not affect VERP in either LQT1 or LMC rabbits (Fig. 3, A and B), the baseline genotype differences in VERP dispersion were abolished under ISO.

To investigate the effect of ISO at the cellular level, we studied its effect on  $I_{Ks}$  densities in cardiomyocytes derived from LQT and LMC rabbits (Fig. 3C). We found a twofold increase in  $I_{Ks}$  densities during ISO in LQT2 [baseline (pA/pF):  $0.65 \pm 0.07$  vs. ISO:  $1.53 \pm 0.16$ ,  $P < 0.05$ ] and LMC [baseline (pA/pF):  $1.12 \pm 0.15$  vs. ISO:  $2.22 \pm 0.57$ ,  $P < 0.05$ ]. These currents were suppressed by consecutive exposure to the  $I_{Ks}$ -blocker chromanol 293B. Thus, like the normal  $I_{Ks}$  currents in LMC myocytes, the attenuated  $I_{Ks}$  currents in LQT2 myocytes (4) remained sensitive to stimulation by ISO. As we reported previously,  $I_{Ks}$  currents were abolished in myocytes derived from LQT1 rabbits (4), in which only a nonspecific response was observed during ISO exposure (Fig. 3C).

**Programmed ventricular stimulation: Lack of inducibility.** Consistent with the rare VT inducibility in human patients with

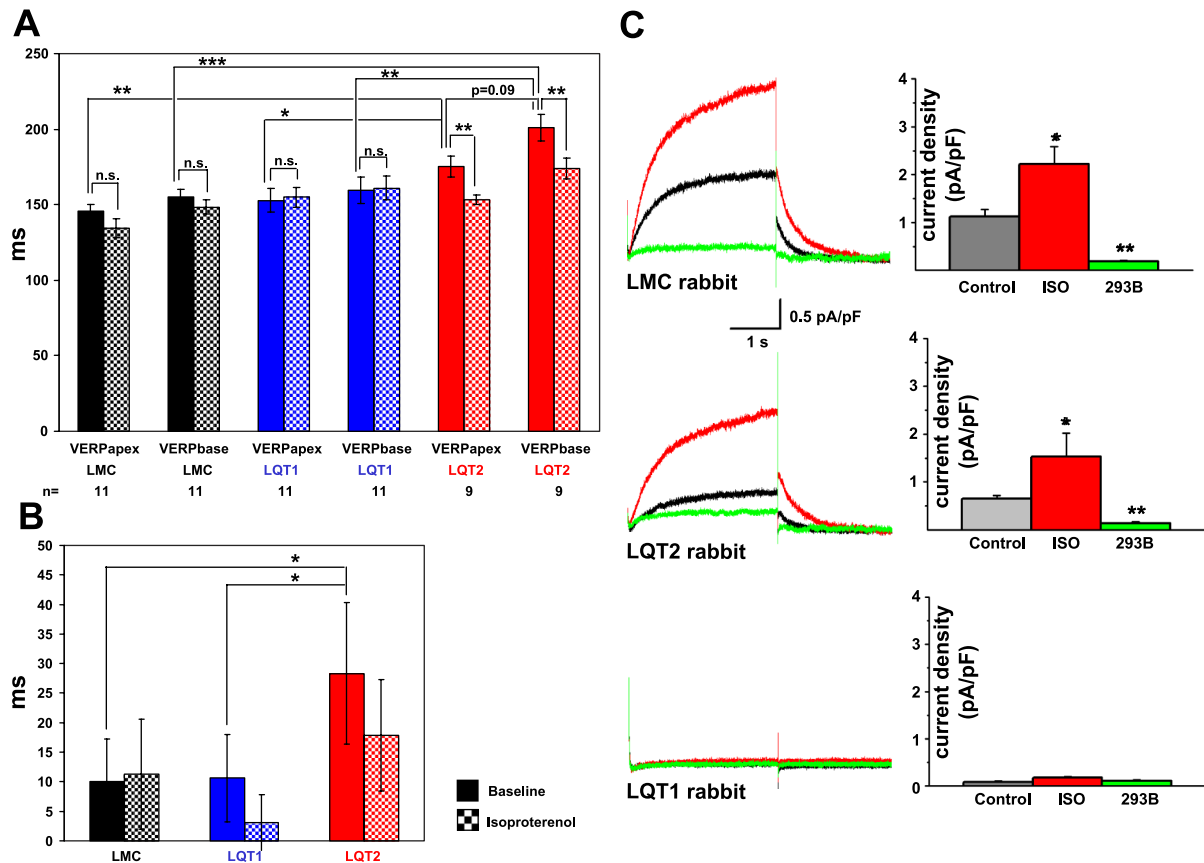


Fig. 3. Ventricular effective refractory period (VERP) dispersion and pharmacogenomic effect of isoproterenol on VERP. A: VERP in RV apex and base (at 240 ms stimulation CL) are shown at baseline (colored bars) and during isoproterenol (checkered bars) in LMC (black), LQT1 (blue), and LQT2 (red) rabbits. All values are presented as means  $\pm$  SD.  $**P < 0.01$ .  $***P < 0.001$ . B: VERP dispersion (ms) in LMC, LQT1, and LQT2 rabbits at baseline (colored bars) and during isoproterenol (checked bars).  $*P < 0.05$ . C: effect of isoproterenol (100  $\mu$ M) on slow delayed-rectifier  $K^+$  current ( $I_{Ks}$ ) densities.  $I_{Ks}$  peak current densities in apical myocytes derived from LMC ( $n = 10$  myocytes), LQT2 ( $n = 10$ ), and LQT1 ( $n = 9$ ) rabbits are shown at baseline control conditions (black line), during isoproterenol administration (ISO, red line), and after blockade with 50  $\mu$ M chromanol 293B (green line). Column on left shows typical recordings from single cells, recorded from holding potential of  $-40$  to  $+30$  mV. Column on right shows quantification of  $I_{Ks}$  current densities (pA/pF) at  $+10$  mV. NS, not significant.  $*P < 0.05$  vs. control conditions.  $**P < 0.01$  vs. ISO.

LQTS (2, 5), none of the LQT2 rabbits and only 1 of 10 LQT1 rabbits was VF inducible via endocardial programmed stimulation with up to three coupled extra stimuli. The induction of sustained pVT in 4 of 11 LMC rabbits strongly suggests the same nonspecificity as in human patients (10).

**Pharmacogenomics: Effect of dofetilide on QT duration and AV conduction.** To assess the different pharmacogenomic effects of the  $I_{K_r}$ -blocker dofetilide (32) on cardiac repolarization as represented by the QT interval, we used genotype-specific heart rate correction formulas to calculate QT<sub>i</sub> (4). Dofetilide markedly prolonged the absolute QT duration (Fig. 4A) and slowed the heart rate in LQT1 rabbits (Fig. 4B), resulting in a markedly increased QT<sub>i</sub> (Fig. 4C). This drug-induced QT<sub>i</sub> prolongation was significantly more pronounced in LQT1 than in LMC animals (Fig. 4C), although dofetilide also significantly prolonged the QT<sub>i</sub> in LMC compared with baseline QT<sub>i</sub>. In contrast, no changes in QT<sub>i</sub> were observed in LQT2 rabbits, indicating that they are insensitive to  $I_{K_r}$  blockers (Fig. 4C). All LQT1 rabbits (8/8) developed complete AV block after dofetilide administration, which facilitated an episode of nonsustained pVT in one LQT1 rabbit (Fig. 4D). During these episodes of complete AV block, the RR intervals ranged from 1,000 to 4,790 ms (corresponding to heart rates of 60–13 beats/min) with QT intervals of the same duration (Fig. 5A). In contrast, none of the LMC or LQT2 rabbits developed AV block under dofetilide (Fig. 5, B and C). All recordings shown in Fig. 5, A–C, were taken 10 min after the bolus administration of dofetilide. In LQT1 rabbits, the RR interval was determined by the duration of the preceding QT interval (Fig. 5A). The inability to pace the ventricle until after the end of the T wave (Fig. 5D) is consistent with markedly prolonged ventricular refractoriness as the cause of dofetilide-induced block in LQT1

rabbits (but does not rule out concurrent block more proximally in the conduction system). In addition, LQT1 rabbits showed a progressive widening of the His bundle electrogram (HBE) within the 1st min after administration of dofetilide. The HBE disappeared upon the onset of the AV block, which consistently appeared within 2 min after the bolus (Fig. 5E). These observations suggest that dofetilide might also have a direct effect on the conduction of the His-Purkinje system in LQT1 rabbits. The steady, progressive change in HBE morphology, the consistent normal HBE before this change (data not shown), and the temporal correlation between the change in HBE and the occurrence of AV block suggest that this is not an artifact due to a change in catheter position.

To further investigate the level of AV block in LQT1 rabbits early after the dofetilide bolus, we performed optical mapping experiments in LQT1, LMC, and LQT2 rabbits at baseline and after dofetilide exposure ( $10^{-9}$  mol/l). Figure 6 shows the experimental set-up (Fig. 6A), a schematic of the  $4 \times 4$ -mm field of view (Fig. 6B), and the typical His signals (Fig. 6C), which are similar to previously reported optical His signals (7, 20). Each of the fluorescence signals from the lower part of the atrium, AVN, and His region consists of two distinct upstrokes/components. The first component depicts the specific signal that corresponds to the atrial action potential, the AVN signal, or the His action potential. The second component depicts the underlying ventricular action potential. To confirm the identity of these signals, we simultaneously recorded signals using a bipolar electrode (Fig. 6, B–D). As shown in Fig. 6C, the atrial signal coincides with the A signal, and the His signal coincides with the H signal of the bipolar electrode. Moreover, we confirmed the location of the His in serial sections of the region of the field of view using immunohistochemical staining with

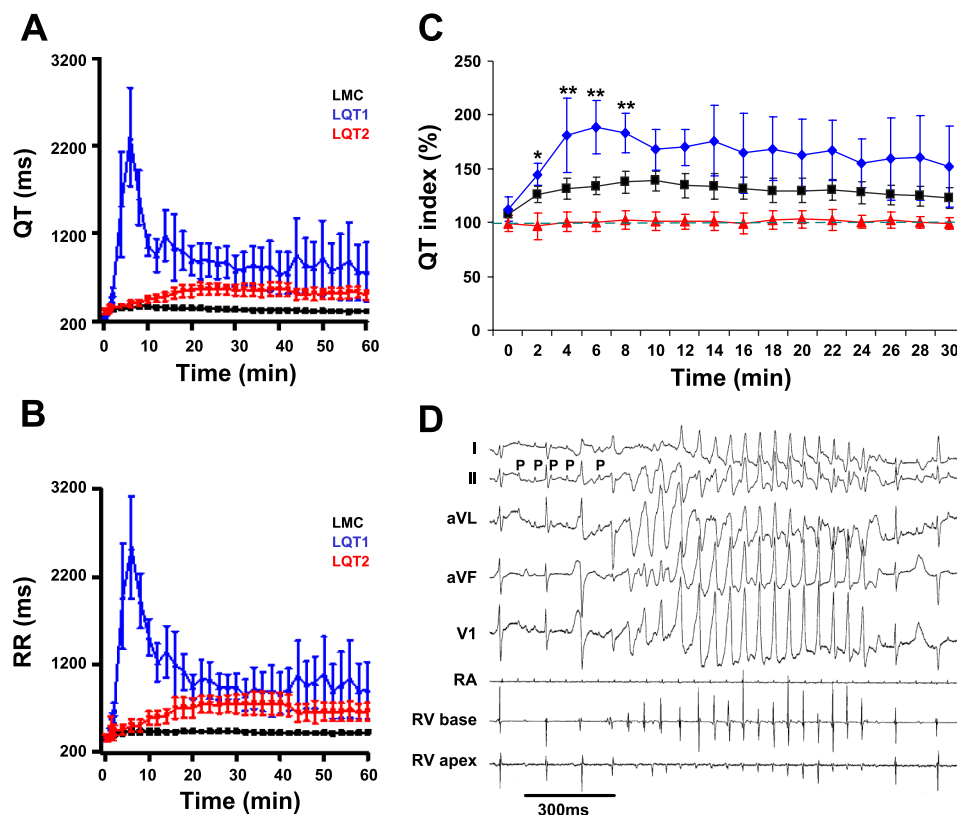


Fig. 4. Pharmacogenomic effect of dofetilide. A: absolute duration of QT vs. time after dofetilide bolus (0.02  $\mu$ g/kg) in LMC (black line), LQT1 (blue line), and LQT2 (red line) rabbits. B: duration of RR vs. time after dofetilide bolus. C: heart rate-corrected QT index (QT<sub>i</sub>) after dofetilide bolus. \* $P < 0.05$  LQT1 vs. LMC. \*\* $P < 0.01$  LQT1 vs. LMC. Green hatched line indicates expected QT<sub>i</sub> (100%). D: episode of dofetilide-induced polymorphic ventricular tachycardia (pVT) in LQT1 male during episode of alternating AV 2:1/3:1 block. P, P wave.

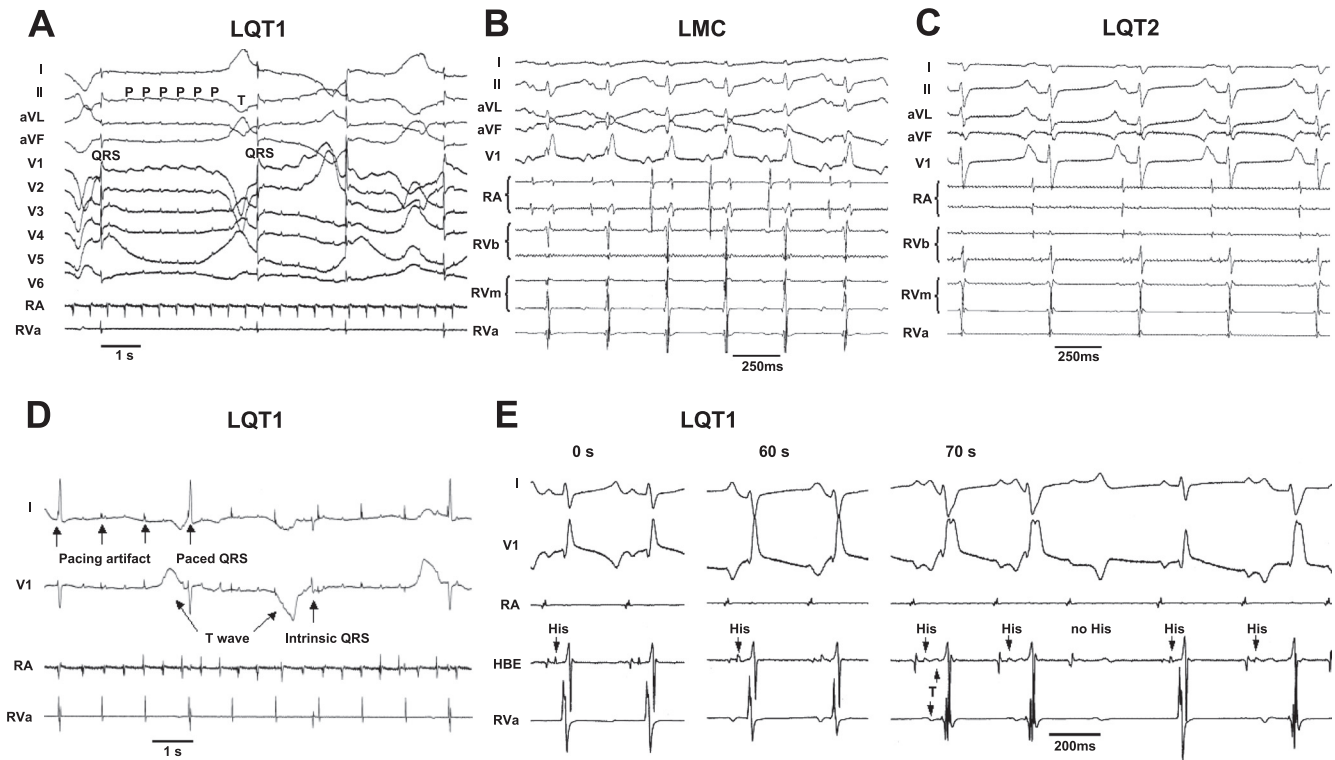


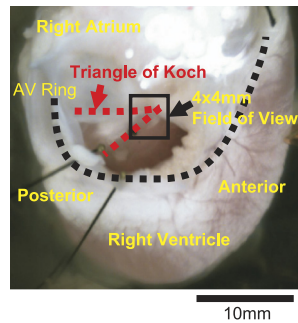
Fig. 5. Effect of dofetilide on AV conduction in LQT1 rabbits. *A*: high-grade AV block (10 min after dofetilide bolus, 0.02  $\mu\text{g}/\text{kg}$ ) shown at slow paper speed. Note that RR interval depends on QT interval. *B*: representative ECG tracing of LMC rabbit under dofetilide showing QT prolongation but absence of AV block (10 min after dofetilide bolus). *C*: representative ECG tracing of LQT2 rabbit under dofetilide: absence of AV block (10 min after dofetilide bolus). *D*: the inability to pace the ventricle in LQT1 rabbit until after the end of the T wave confirms ventricular refractoriness. Note the T wave alternans. *E*: His bundle recordings (indicated by arrows) in LQT1 rabbit at baseline and 60 and 70 s after dofetilide bolus. Progressive decrease in amplitude of the His electrogram is seen 60 s after dofetilide bolus. At 70 s, there is a further decrease in amplitude and an increase in duration of the His, infra-His conduction delay with QRS widening, and then a second-degree AV block.

anti-neurofilament 70 antibodies (Fig. 6E, *i-iii*). Of note, we estimate the diameter of the bundle of His on histochemistry to be 0.7 mm, whereas on optical mapping it measures 1.3–1.5 mm. This near doubling of the His size is likely because of overestimation in optical mapping from spatial averaging and signal scatter as well as underestimation in the neurofilament 70-stained tissue due to dehydration and shrinkage of the His bundle during sample preparation.

We calculated the CV of the His bundle by plotting the activation time against the distance along the AV junction/His region. We found two regions with different conduction: first a region with slow conduction (long activation time), corresponding to the AV node (labeled “a” in Fig. 6Eii), followed by a region with fast conduction (short activation time), which we designated the physiological His region (labeled “b” in Fig. 6Eii). Histological evidence of His tissue was found in *region b* (Fig. 6Eiii). To further characterize the His conduction at baseline, we measured AH and HV intervals and progressively shortened the atrial pacing cycle length until we reached Wenckebach behavior or 2:1 AV block (Table 2), similar to the *in vivo* EPS experiments. Of note, the HV intervals measured in this preparation were longer than during the *in vivo* EPS, since the ventricular signal in the bipolar electrode in this set-up occurs later (during depolarization of the septum) than in the EPS, where by definition the earliest ventricular signal in any intracardiac electrode was used to measure the HV interval. During progressively faster atrial pacing, we observed a block at the AVN level at a CL of  $227 \pm 21$  ms, which

was slower than *in vivo* due to the lack of sympathetic innervation and circulating catecholamines in the Langendorff-perfused heart preparation. In LQT1 rabbits, the mean His CV (baseline:  $0.66 \pm 0.14$  m/s) was significantly reduced by dofetilide ( $0.39 \pm 0.04$  m/s,  $n = 5$ ,  $P < 0.05$ ). Moreover, the Wenckebach CL was significantly prolonged compared with baseline ( $P < 0.001$ , Table 2). We also noted a persistent 2:1 AV conduction block in all five LQT1 hearts at a stimulation CL of 400 ms, with a loss of the sharp His deflection in the bipolar HBE (Fig. 7A) on alternating atrial depolarizations, and no conduction to the ventricle. This change in His deflection mimics the bipolar electrode recordings early after *in vivo* bolus administration of dofetilide in LQT1 rabbits (Fig. 5E). However, the bipolar electrode in this experimental setting was placed at a distal location, since no optical signals could be registered if the electrodes were placed exactly on the His. Consequently, the His signal in the bipolar HBE nearly disappears during the block. The simultaneously acquired optical signals showed alternating His signal morphology (Fig. 7B). The first conducted beat (Fig. 7B) shows normal His conduction with a sharp upstroke of the His signal of the conducted beat in all His locations (C1–C5), starting from the proximal area (C1) located near the AV node (with some overlap of nodal signal) through the distal His area (C5). The second (blocked) beat shows progressively altered His morphology with gradual slowing of the upstroke of His signal, from His locations 2 to 4. No discernible signal  $dF/dt$  above noise level ( $90 \pm 64$  U/ms) is seen in His location 5

**A** Perfused AV Node Preparation



**B** Schematic of optical mapping field of view

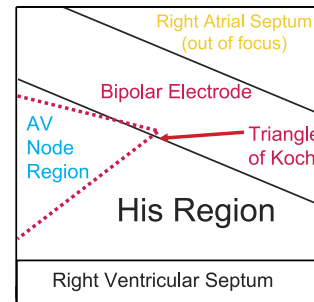
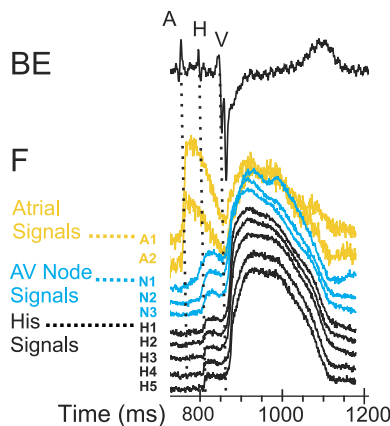
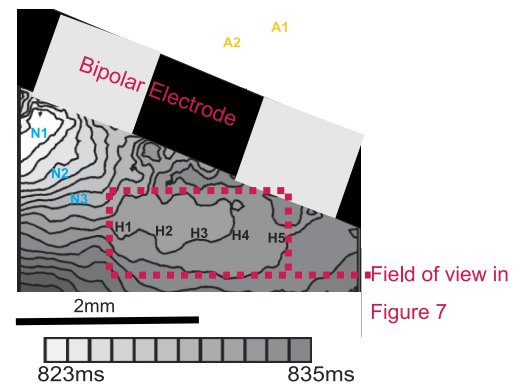


Fig. 6. *A*: perfused AV node preparation. *B*: schematic of the optical mapping 4 × 4-mm field of view. *C*: bipolar HBE (BE) and optical mapping signals (F) in atrial region (yellow), AV node region (light blue), and His region (black) within the 4 × 4-mm field of view. Dotted lines delineate the concordance of the optical signals with the bipolar signals A (atrium), H (His), and V (ventricle). *D*: activation maps of AV node and His signals. Regions labeled A1 and -2, N1-3, and H1-5 demonstrate points from which signals shown in *C* were obtained. The field of view of the activation maps shown in Fig. 7, *C* and *D*, is indicated by a red square. *E*: AV junction activation map (*i*) and corresponding time plot (*ii*). The red broken line indicates the line drawn from the AV junction toward the end of the His activation, along which we plotted the activation time. Relative activation time is plotted against the distance within the AV junction. “a” indicates region with slow conduction, corresponding to AV node; “b” indicates region with fast conduction, corresponding to His. *iii*, Immunohistochemical staining of the region corresponding to the optical mapping field of view; Masson’s Trichrome (*top*) and immunohistochemical staining with anti-Neurofilament-70 antibody (*bottom*).

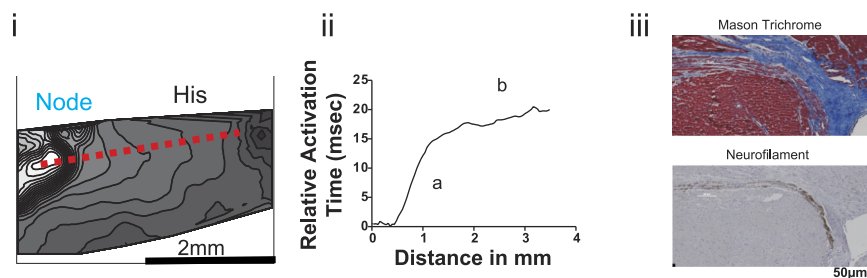
**C** Recordings in 4x4 field of view



**D** Activation map of AV node and His signals



**E** AV Junction activation map with corresponding time plot and histology of a perpendicular section through the region in activation map



(labeled B5 in Fig. 7B). Moreover, in the activation maps (Fig. 7, C and D), a block within the path of the His signal could be seen between locations 4 and 5 (Fig. 7D). At location 5 and beyond there is loss of the smooth activation map isochronal lines because of the loss of the His signal and resulting errors

in the automatic detection of  $dF/dt$ . This finding suggests a dofetilide-induced intra-His block. To further illustrate the block, we show the activation time plots of consecutive conducted and blocked beats along the same red dashed line depicted in Fig. 7E. On conducted beats, the same regions of

Table 2. His conduction parameters in AVN/His preparation

	Baseline				Dofetilide				
	AH, ms	HV, ms	AV/His-WCL, ms	Block at AVN	AH, ms	HV, ms	AV/His-WCL, ms	Block at AVN	Block Intra-His
LMC	51 ± 14	45 ± 4	253 ± 23	3/3	64 ± 18	43 ± 3	310 ± 36 <sup>b</sup>	2/3	0/3
LQT1	56 ± 7	40 ± 4	227 ± 21	5/5	63 ± 5	42 ± 6	480 ± 36 <sup>c</sup>	0/5	5/5 <sup>d</sup>
LQT2	59 ± 5	42 ± 3	363 ± 18 <sup>a</sup>	2/3	79 ± 22	45 ± 3	406 ± 87	2/3	0/3

Values are presented as means ± SD. AVN, AV node. <sup>a</sup>*P* < 0.05 vs. LQT1. <sup>b</sup>*P* = 0.08 vs. LMC baseline. <sup>c</sup>*P* < 0.001 vs. LQT1 baseline. <sup>d</sup>*P* < 0.05 vs. LMC and LQT2.

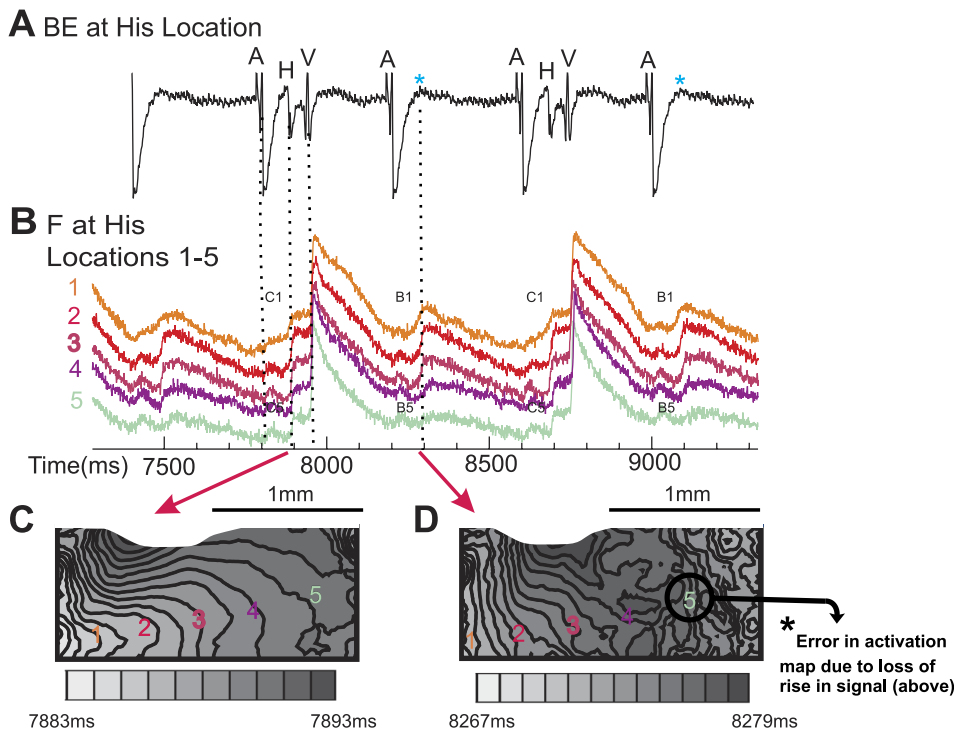
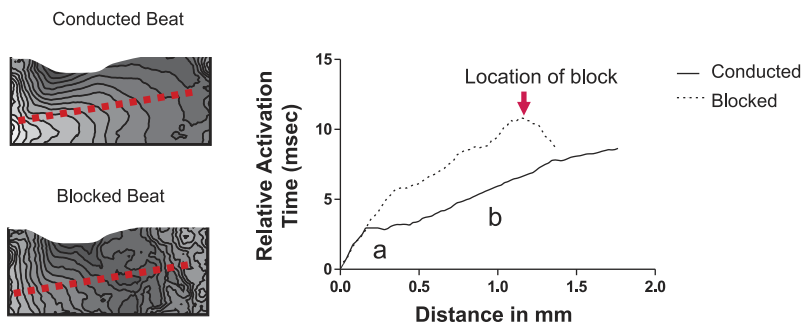


Fig. 7. A: bipolar electrode signals (BE) at the His location during continuous dofetilide perfusion ( $10^{-9}$  mol/l) showing 2:1 block. The light blue asterisk marks the lack of sharp His deflection upon AV conduction block. B: optical signals (F) from very proximal His location 1 to distal location 5 as indicated in the activation maps below. C1 and C5 indicate the normal His signals of the conducted (C) beat at positions 1 and 5, respectively. B1 and B5 indicate the signals of the blocked (B) beat at positions 1 and 5, respectively. B1 depicts normal His signal at the proximal His, whereas B5 indicates the loss of detectable activation (dF/dt) above noise level at location 5 distal to the intra-His block. C and D: activation map at the His location (indicated are the locations 1–5) of the conducted beat (C) and of the blocked beat (D) as indicated by the red arrows. The size of the optical field is 4 mm (x-axis)  $\times$  2 mm (y-axis). Time scale is identical to the time scale in B. The gray scale under the activation maps indicates the different times of the activation. Note the closer spacing of isochronal lines in the activation map of the blocked beat, consistent with slower His conduction. At the blocked beat, at location 5 and beyond, there is loss of smooth activation isochronal lines due to loss of signal. E: AV junction activation maps and time plots for conducted and blocked beats post-dofetilide in LQT1. The red dashed line indicates the line along which we plotted the activation time. Relative activation time is plotted against the distance within the AV junction with slower conduction of the blocked beat (broken line) than the conducted beat (solid line) in the His region (labeled “b”) and, finally, the premature termination of the conduction of the blocked beat.

**E** AV Junction activation maps and time plots for even and odd beats post dofetilide in LQT1



slow (AV nodal) and fast (His) conduction are seen as described at baseline. On blocked beats, again, the same two-phase plot is seen, with slower conduction in the His region (labeled “b”) and, finally, the premature termination of the conduction at the location of the block. Importantly, the block occurs within the more rapid conduction (flatter slope) of the activation plot, suggesting termination of the activation time plot at the proximal His region. Thus, we conclude that block occurs at the proximal His level. The change in His signal morphology and activation map isochronal line spacing between conducted and nonconducted beats demonstrates a persistent beat-to-beat alternating pattern. Fluorescence signals demonstrated prolongation of the ventricular action potential duration (APD): pre-dofetilide  $269 \pm 35$  ms vs. post-dofetilide  $313 \pm 56$  ms,  $n = 5$ ,  $P < 0.05$ , paired  $t$ -test. However, the His signal of the nonconducted second beat occurred clearly after full ventricular repolarization, suggesting that ventricular tissue should have fully recovered from refractoriness and should initiate action potentials if activation is delivered through the

His during this time period (Fig. 7B). Of note, the APD of the different regions within the His at baseline and during dofetilide perfusion cannot be measured, since only the depolarization and the initial phase of the repolarization of the His are discernible; the majority of the repolarization of the His is hidden by the large ventricular action potential, as shown in Figs. 6C and 7B. At higher concentrations of dofetilide ( $10^{-8}$  mol/l), we observed pseudo-AV blocks due to pronounced prolongation of the ventricular APD, similar to the in vivo observation later after the dofetilide bolus.

In LMC and LQT2 rabbit tissue, the baseline mean His CV was similar to LQT1 tissue, with a trend toward a slower CV in LQT2 (LMC,  $0.60 \pm 0.09$  m/s,  $n = 3$ ; LQT2,  $0.54 \pm 0.04$  m/s,  $n = 3$ ). AH and HV intervals were not significantly different from LQT1 hearts (Table 2). However, Wenckebach behavior occurred at significantly longer CL in LQT2 compared with LQT1 hearts ( $P < 0.05$ ) and tended to be longer in LQT2 than in LMC ( $P = 0.08$ ), with the block occurring at the AVN level in all LMC, all LQT1, and 2/3 LQT2 hearts. In one LQT2 rabbit, the block

occurred below the His, corresponding to the infra-His block in LQT2 rabbits observed during the *in vivo* EPS. Of note, similarly as in LQT1 heart preparations, Wenckebach behavior occurred at longer CL than *in vivo* in LQT2 and LMC hearts because of the lack of sympathetic innervations and circulating catecholamines in the Langendorff-perfused heart preparation. In contrast to LQT1 rabbits, the mean His CV was not significantly changed by dofetilide (LMC,  $0.58 \pm 0.20$  m/s,  $n = 3$ ; LQT2,  $0.51 \pm 0.08$  m/s,  $n = 3$ ) (Fig. 8, A and B). Moreover, the same concentration of dofetilide ( $10^{-9}$  mol/l) did not cause conduction blocks within the His in either LMC or LQT2 rabbits at the stimulation CL of 400 ms. Figure 8 presents activation maps and activation time plots in LMC (Fig. 8A) and LQT2 (Fig. 8B), showing no beat-to-beat change in conduction through the region under dofetilide, indicating that a combined block of  $I_{Kr}$  (by dofetilide) and  $I_{Ks}$  (absent in LQT1) may be necessary to disrupt His conduction. Further

shortening of the stimulation cycle length, however, caused AV Wenckebach behavior and 2:1 AV block, which occurred in the AV nodal region in 2/3 LMC and 2/3 LQT2 and at the infra-His level in 1/3 LMC and 1/3 LQT2 hearts but never within the His region. During dofetilide infusion, Wenckebach CL was significantly prolonged in LQT1 ( $P < 0.001$ ) and tended to be prolonged in LMC ( $P = 0.08$ ), but was not significantly changed in LQT2 hearts (Table 2).

## DISCUSSION

*In vivo EP study.* Here we show for the first time the feasibility of detailed *in vivo* transvenous catheter-based EPS, including His signals, in anesthetized rabbits and elucidate the differences in the impact of the loss of  $I_{Ks}$  or  $I_{Kr}$  on AV/His conduction and spatial dispersion of refractoriness (DR) in the

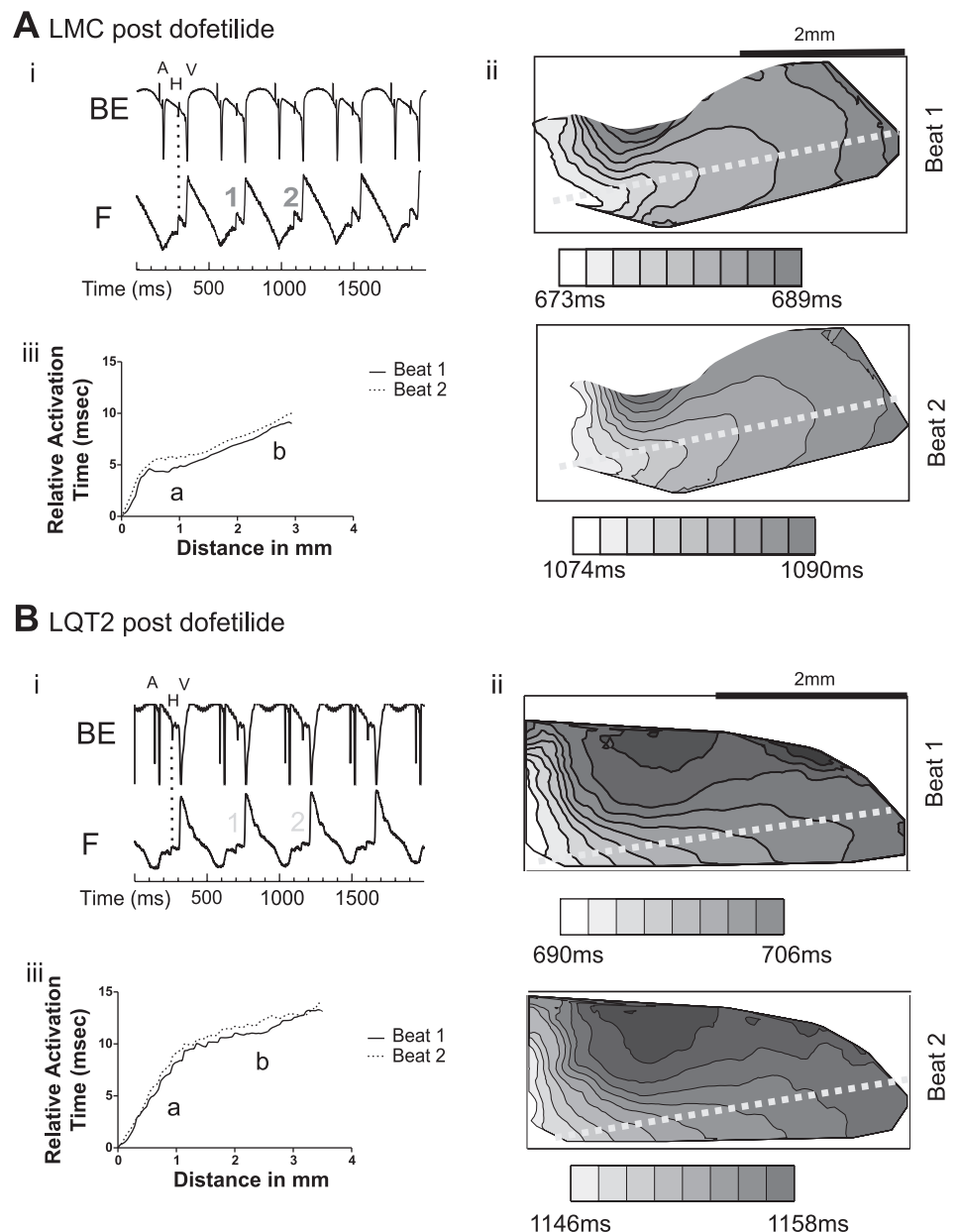


Fig. 8. AV conduction in LMC and LQT2 rabbits during continuous dofetilide perfusion ( $10^{-9}$  mol/l). A: LMC. B: LQT2. *i*, Sample traces of His bipolar electrograms (BE) and fluorescence optical recordings (F). Broken lines delineate the concordance of the optical signals with the bipolar signals A, H, and V. *ii*, Activation maps through the AV node (AVN)/His junction of two consecutive beats (*beat 1* and *beat 2*). The field of view was set to  $2 \times 4$  mm<sup>2</sup>, and the isochronal lines were drawn at 2-ms intervals, with darker color indicating later activation. *iii*, Relative activation time plots for consecutive *beats 1* and *2*. Both groups showed distinct His bipolar electrograms, distinct His upstrokes in the optical signals, and His conduction without block under dofetilide in contrast to the LQT1 group shown in Fig. 7.

RV. Thus far, reports of in vivo EPS of anesthetized rabbits have been limited to the characterization of ventricular refractory periods or arrhythmias by placement of electrodes on the right ventricular epicardial surface after sternotomy (28, 41). Although the heart rate of rabbits is significantly faster (200–300 beats/min) than that of humans and, in turn, all electrophysiological parameters are shorter, the ratios of the duration of these parameters (i.e., AH, HV, AERP, AVNERP, VERP) to sinus CL in wild-type rabbits are similar to those described as normal values in humans (38).

*VERP, VERP dispersion, and differential effects of ISO.* We observed a longer VERP in LQT2 than in LMC and LQT1 rabbits, a prolongation that correlated with the longer QT intervals in free-moving LQT2 than in LMC rabbits (4). In contrast, VERP was not longer in LQT1 than in LMC rabbits, despite the significantly prolonged QT intervals in free-moving LQT1 rabbits (4). These discrepancies between findings in free-moving rabbits and rabbits under anesthesia stem from the use of the  $I_{Ks}$ -blocker isoflurane, which prolongs the QT only in LQT2 and LMC but not in LQT1 rabbits (29), creating a drug-induced LQT1 phenotype in LMC rabbits, thereby reducing the baseline differences in cardiac repolarization between LQT1 and LMC rabbits. In addition, we found a more pronounced VERP dispersion between the base and apex of the RV endocardium in LQT2 than in LQT1 or LMC rabbits. These observations in the RV endocardium are in line with the greater spatial APD dispersion in the LV epicardium in LQT2 than in LQT1 or LMC rabbits (4) and thus suggest a higher DR involving the entire heart in LQT2 rabbits. ISO, which increased  $I_{Ks}$  densities in LQT2 and LMC, decreased the VERP dispersion in LQT2 rabbits by shortening the VERP more pronouncedly in the RV base, suggesting that the DR is dynamically controlled by the distribution and likely differential post-translational modifications of  $I_{Ks}$  pre- and post-sympathetic stimulation. Obviously, additional currents such as voltage-sensitive L-type calcium current may also play a role in regulating VERP and VERP dispersion.

*His block in LQT2 rabbits under isoflurane and in LQT1 rabbits under dofetilide.* Both LQT1 and LQT2 rabbits showed AV conduction block when exposed to  $I_{Kr}$  or  $I_{Ks}$  blocking drugs such as dofetilide (LQT1) and isoflurane (LQT2), respectively. The occurrence of AV conduction block during  $I_{Ks}$  blockade only in LQT2 and during  $I_{Kr}$  blockade only in LQT1 rabbits indicates genotypic differences in the susceptibility of the conduction system to  $I_{Kr}$ - or  $I_{Ks}$ -blockade, respectively. However, the levels of the AV conduction blocks differed. In LQT2 rabbits (with genetically abolished  $I_{Kr}$  and partly blocked  $I_{Ks}$  due to isoflurane), we demonstrated infra-His 2:1 block, whereas LQT1 rabbits (with genetically abolished  $I_{Ks}$  and partly blocked  $I_{Kr}$  due to dofetilide) showed higher-grade AV block as a result of a markedly prolonged ventricular refractoriness, termed pseudo-AV block (35). Moreover, the progressive prolongation of the duration of His potential, the decrease in the amplitude of the His potential, and the eventual disappearance of the His signal upon AV conduction block early after dofetilide administration suggested an additional effect on the His-Purkinje system. Indeed, ex vivo optical mapping studies in LQT1 rabbits demonstrated a dofetilide-induced slowing of His conduction velocity and 2:1 intra-His block (proximal His), despite a fully repolarized ventricle, whereas no such block was observed in either LMC or LQT2

rabbits. One may speculate that the delayed conduction and the intra-His block in LQT1 hearts may be, at least partly, due to a prolonged repolarization in the His-Purkinje system. However, it is unfortunately impossible to measure APD of the His with current optical mapping techniques, since only the depolarization and the initial phase of the repolarization of the His are discernible while the majority of the repolarization of the His is hidden by the large ventricular action potential, as shown in Fig. 6C. The baseline His conduction velocities measured in LMC and LQT1 rabbits are comparable to His CV described in humans (0.8 m/s) (19). The baseline His CV tended to be slower in LQT2 than in LQT1 rabbits, indicating that a baseline difference may contribute to the pronounced genotype difference in His conduction (HV, His-Wenckebach CL, and His-ERP) between LQT2 and LQT1 rabbits under isoflurane anesthesia.

Of note, our technique of CV measurement of the His relies on His activation parallel to the AV junction surface. Although this is usually the case with the proximal His, the more distal His is buried deeper in the myocardium and may therefore become oblique to the surface. In such case, the His CV would be underestimated by our technique. While this may alter our absolute measurements of His CV, we expect that it would not change the response to dofetilide in LQT1 hearts and could not produce the beat-to-beat changes in CV and intra-His conduction block that we observed. The conduction system abnormalities seen in LQT1 and LQT2 rabbits highlight the role of the delayed-rectifier potassium currents in the AV junction/His-Purkinje system. So far, no studies have explored the effect of HERG or KvLQT1 mutations on His-Purkinje APD and His-Purkinje conduction directly, although both HERG and KvLQT1 are expressed in Purkinje cells (8, 17), and Purkinje fibers are a well-established, sensitive system in the preclinical evaluation of QT-prolonging effects of  $I_{Kr}$ -blocking drugs (15). Moreover, rabbit Purkinje fibers have been determined to be even more sensitive than ventricular myocytes for detecting  $I_{Kr}$ -blocker-induced APD prolongations and EADs (26).

We observed an infra-His block (i.e., with no change in His signal morphology) in LQT2 rabbits exposed to  $I_{Ks}$  blockers but proximal intra-His block in LQT1 rabbits exposed to  $I_{Kr}$  blockers, with a widening of the HBE and a slowing of His conduction. These distinct types of block suggest a differential role of  $I_{Kr}$  and  $I_{Ks}$  in different areas of the rabbit His-Purkinje system that lead to a differential regional sensitivity of the His-Purkinje system to  $I_{Kr}$ - and  $I_{Ks}$ -blocking drugs. We speculate that differential expression of  $I_{Kr}$  and  $I_{Ks}$  in the proximal His and the distal His-Purkinje system may underlie this regionally different sensitivity. However, to date, no studies have compared the relative distribution of  $I_{Kr}$  and  $I_{Ks}$  in different parts of the His-Purkinje system.

*Clinical implications: AV conduction blocks and pharmacogenomic effects of  $I_{Kr}$  and  $I_{Ks}$  blockers.* Recently, it has been demonstrated that the His-Purkinje system plays a crucial role in triggering polymorphic VT in LQTS (1). Moreover, in LQT2 patients, AV conduction blocks, which likely occur on the infra-His level as demonstrated here in LQT2 rabbits, are a proven trigger for pVT (36). Similarly, spontaneous AV conduction blocks preceded episodes of pVT in several free-moving, nonanesthetized LQT2 rabbits (4). Consequently, drugs that affect His-Purkinje conduction and refractoriness and hence exaggerate these AV conduction abnormalities

likely have a major effect on arrhythmogenesis in LQTS. We demonstrate differential pharmacogenomic effects of  $I_{Kr}$  or  $I_{Ks}$  blockers on His-Purkinje conduction in LQT rabbits, indicating that the rarely described true infranodal AV blocks in LQTS patients (16, 31) may be more frequent when LQT2 patients are exposed to  $I_{Ks}$  blockers and, moreover, that these  $I_{Ks}$ -blocker-induced AV conduction blocks may increase the risk for arrhythmias in LQT2. Indeed, we have previously shown that  $I_{Ks}$ -blocker-induced AV conduction blocks initiated pVT in LQT2 rabbits (29). Similarly, because the dofetilide-induced intra-His block in LQT1 rabbits occurs at pronouncedly lower dofetilide levels than the dofetilide-induced complete AV block that were observed in wild-type rabbits, without further investigation of the level of the block (24), we suspect that the risk for His block with  $I_{Kr}$ -blocking drugs such as dofetilide might be significantly increased in patients with underlying KvLQT1 mutations, despite the relative rarity of AV conduction block with dofetilide in the general population (0.4–1.5%, according to dofetilide product information; Pfizer). These observations suggest that it may be clinically important to genotype LQT patients or undiagnosed patients with prolonged heart rate corrected QT interval duration when treatment with drugs or anesthetic agents that modulate the function of either  $I_{Kr}$  or  $I_{Ks}$  channels is considered. However, since we assessed the effects of  $I_{Ks}$ - and  $I_{Kr}$ -blocking drugs in models with pore mutants of KvLQT1 or HERG that completely lack  $I_{Ks}$  or  $I_{Kr}$ , the side effects of these drugs might be more subtle and remain to be elucidated in subjects with mutations that have a less pronounced QT prolongation.

**Limitation of the study.** The in vivo EPS were performed using the  $I_{Ks}$ -blocking drug isoflurane for anesthesia because of the lack of suitable alternative anesthetic drugs without QT-prolonging effects but sufficient analgesic properties. However, due to its  $I_{Ks}$ -blocking properties, isoflurane creates a drug-induced LQT1 phenotype in LMC rabbits, resulting in QT<sub>i</sub> and VERP prolongation and hence may abolish potential differences between LQT1 and LMC rabbits, limiting the comparison between the LQT1 and LMC data.

In conclusion, intracardiac transvenous in vivo EPS are feasible in rabbits and allow detailed analysis of electrophysiological parameters, including spatial differences of refractory periods, His bundle signals, and the discrimination of level of AV conduction block.

We observed genotypic differences in spatial DR, with the most pronounced DR in LQT2 rabbits. ISO decreased the DR in LQT2 but did not affect the smaller DR in LQT1 rabbits. Moreover, we demonstrated different levels of AV conduction blocks in LQT1 and LQT2 rabbits during exposure to  $I_{Kr}$ - or  $I_{Ks}$ -blocking drugs with infra-His blocks in LQT2 rabbits under isoflurane and a slowing of His-Purkinje conduction and intra-His block in LQT1 rabbits under dofetilide, suggesting differential regional sensitivities of the His-Purkinje system to drugs that modulate  $I_{Kr}$  or  $I_{Ks}$  channels.

#### ACKNOWLEDGMENTS

We thank Alfred E. Buxton for valuable comments in reviewing the manuscript.

#### GRANTS

G. Koren is the recipient of National Heart, Lung, and Blood Institute Grant RO1 HL-046005-14; K. E. Odening was supported in part by grants from the

German Cardiac Society (St. Jude Medical Stipendium) and the German Research Foundation (DFG Forschungsstipendium) and is currently supported by an American Heart Association postdoctoral fellowship award.

#### DISCLOSURES

No conflicts of interest are declared by the authors.

#### REFERENCES

1. Ben Caref E, Boutjdir M, Himel HD, El-Sherif N. Role of subendocardial Purkinje network in triggering torsade de pointes arrhythmia in experimental long-QT syndrome. *Europace* 10: 1218–1223, 2008.
2. Bhandari AK, Shapiro WA, Morady F, Shen EN, Mason J, Scheinman MM. Electrophysiologic testing in patients with the long-QT syndrome. *Circulation* 71: 63–71, 1985.
3. Brunner M, Guo W, Mitchell GF, Buckett PD, Nerbonne JM, Koren G. Characterization of mice with a combined suppression of  $I_{to}$  and  $I_{Ks,slow}$ . *Am J Physiol Heart Circ Physiol* 281: H1201–H1209, 2001.
4. Brunner M, Peng X, Liu GX, Ren XQ, Ziv O, Choi BR, Mathur R, Hajjiri M, Odening KE, Steinberg E, Folco E, Pringa E, Centracchio J, Macharzina R, Donahay T, Schofield L, Rana N, Kirk M, Mitchell G, Poppas A, Zehender M, Koren G. Mechanisms of cardiac arrhythmias and sudden death in transgenic rabbits with long-QT syndrome. *J Clin Invest* 118: 2246–2259, 2008.
5. Buxton AE, Josephson ME. Role of electrophysiologic studies in identifying arrhythmogenic properties of antiarrhythmic drugs. *Circulation* 73: II-67–II-72, 1986.
6. Choi BR, Jang W, Salama G. Spatially discordant voltage alternans cause wavebreaks in ventricular fibrillation. *Heart Rhythm* 4: 1057–1068, 2007.
7. Choi BR, Salama G. Optical mapping of atrioventricular node reveals a conduction barrier between atrial and nodal cells. *Am J Physiol Heart Circ Physiol* 274: H829–H845, 1998.
8. Cordeiro JM, Spitzer KW, Giles W. Repolarizing K<sup>+</sup> currents in rabbit heart Purkinje cells. *J Physiol* 508: 811–823, 2000.
9. Curran ME, Splawski I, Timothy KW, Vincent GM, Green ED, Keating MT. A molecular basis for cardiac arrhythmia: HERG mutations cause long-QT syndrome. *Cell* 80: 795–803, 1995.
10. DiCarlo LA Jr, Morady F, Schwartz AB, Shen EN, Baerman JM, Krol RB, Scheinman MM, Sung RJ. Clinical significance of ventricular fibrillation-flutter induced by ventricular programmed stimulation. *Am Heart J* 109: 959–963, 1985.
11. Donger C, Denjoy I, Berthet M, Neyroud N, Cruaud C, Bannaceur M, Chivoret G, Schwartz K, Coumel P, Guicheney P. KvLQT1 C-terminal mutation causes a forme fruste long-QT syndrome. *Circulation* 96: 2778–2781, 1997.
12. Ewen A, Archer DP, Samanani N, Roth SH. Hyperalgesia during sedation: effects of barbiturates and propofol in the rat. *Can J Anaesth* 42: 532–540, 1995.
13. Fedorov VV, Lozinsky IT, Sosunov EA, Anyukhovskiy EP, Rosen MR, Balke CW, Efimov IR. Application of blebbistatin as an excitation-contraction uncoupler for electrophysiologic study of rat and rabbit hearts. *Heart Rhythm* 4: 619–626, 2007.
14. Garson A Jr, Dick M 2nd, Fournier A, Gillette PC, Hamilton R, Kugler JD, van Hare GF 3rd, Vetter V, Vick GW 3rd. The long-QT syndrome in children. An international study of 285 patients. *Circulation* 87: 1866–1872, 1993.
15. Gintant GA, Limberis JT, McDermott JS, Wegner CD, Cox BF. The canine Purkinje fiber: an in vitro model system for acquired long-QT syndrome and drug-induced arrhythmogenesis. *J Cardiovascular Pharmacol* 37: 607–618, 2001.
16. Gorgels AP, Al Fadley F, Zaman L, Kantoch MJ, Al Halees Z. The long-QT syndrome with impaired atrioventricular conduction: a malignant variant in infants. *J Cardiovasc Electrophysiol* 9: 1225–1232, 1998.
17. Han W, Bao W, Wang Z, Nattel S. Comparison of ion-channel subunit expression in canine cardiac Purkinje fibers and ventricular muscle. *Circ Res* 91: 790–797, 2002.
18. Horigome H, Nagashima M, Sumitomo N, Yoshinaga M, Ushinohama H, Iwamoto M, Shiono J, Ichihashi K, Hasegawa S, Yoshikawa T, Matsunaga T, Goto H, Waki K, Arima M, Takasugi H, Tanaka Y, Tauchi N, Ikoma M, Inamura N, Takahashi H, Simizu W, Horie M. Clinical characteristics and genetic background of congenital long-QT syndrome diagnosed in fetal, neonatal, and infantile life. A nationwide questionnaire survey. *Jpn Circ Arrhythm Electrophysiol* 3: 10–17, 2010.

19. **Hucker WJ, Fedorov VV, Foyil KV, Moazami N, Efimov IR.** Images in cardiovascular medicine. Optical mapping of the human atrioventricular junction. *Circulation* 117: 1474–1477, 2008.
20. **Hucker WJ, Sharma V, Nikolski VP, Efimov IR.** Atrioventricular conduction with and without AV nodal delay: two pathways to the bundle of His in the rabbit heart. *Am J Physiol Heart Circ Physiol* 293: H1122–H1130, 2007.
21. **Ko YS, Yeh HI, Ko YL, Hsu YC, Chen CF, Wu S, Lee YS, Severs NJ.** Three-dimensional reconstruction of the rabbit atrioventricular conduction axis by combining histological, desmin, and connexin mapping data. *Circulation* 109: 1172–1179, 2004.
22. **Lengyel C, Varro A, Tabori K, Papp JG, Baczko I.** Combined pharmacological block of I(Kr) and I(Ks) increases short-term QT interval variability and provokes torsades de pointes. *Br J Pharmacol* 151: 941–951, 2007.
23. **London B, Jeron A, Zhou J, Buckett P, Han X, Mitchell GF, Koren G.** Long QT an ventricular arrhythmias in transgenic mice expressing the N terminus and first terminus and first transmembrane segment of a voltage-gated potassium channel. *Proc Natl Acad Sci USA* 95: 2926–2931, 1998.
24. **Lu HR, Remeysen P, Somers K, Saels A, De Clerck F.** Female gender is a risk factor for drug-induced long QT and cardiac arrhythmias in an in vivo rabbit model. *J Cardiovasc Electrophysiol* 12: 538–545, 2001.
25. **Lu HR, Vlamincx E, Van Ammel K, De Clerck F.** Drug-induced long QT in isolated rabbit Purkinje fibers: importance of action potential duration, triangulation and early afterdepolarizations. *Eur J Pharmacol* 452: 183–199, 2002.
26. **Lu HR, Vlamincx E, Teisman A, Gallacher DJ.** Choice of cardiac tissue plays an important role in the evaluation of drug-induced prolongation of the QT interval in vitro in rabbit. *J Pharmacol Toxicol Methods* 52: 90–105, 2005.
27. **Lupoglazoff JM, Denjoy I, Villain E, Fressart V, Simon F, Bozio A, Berthet M, Benammar N, Hainque B, Guicheney P.** Long-QT syndrome in neonates: conduction disorders associated with HERG mutations and sinus bradycardia with KCNQ1 mutations. *J Am Coll Cardiol* 43: 826–830, 2004.
28. **McLachlan CS, McGuire MA.** Characterization and incidence of inducible monomorphic ventricular tachycardia in a postinfarction rabbit model. *J Electrocardiol* 40: 89–93, 2007.
29. **Odening KE, Hyder O, Chaves L, Schofield L, Brunner M, Kirk M, Zehender M, Peng X, Koren G.** Pharmacogenomics of anesthetic drugs in transgenic LQT1 and LQT2 rabbits reveal genotype-specific differential effects on cardiac repolarization. *Am J Physiol Heart Circ Physiol* 295: H2264–H2272, 2008.
30. **Patel C, Narayanaswamy S, Medina-Ravell VA, Yan GX.** A rare cause of 2:1 AV block: long QT syndrome (Abstract). *J Cardiovasc Electrophysiol* 19: 990, 2008.
31. **Pruvot E, De Torrente A, De Ferrari GM, Schwartz PJ, Goy JJ.** Two-to-one AV block associated with the congenital long-QT syndrome. *J Cardiovasc Electrophysiol* 10: 108–113, 1999.
32. **Rasmussen HS, Allen MJ, Blackburn KJ, Butrous GS, Dalrymple HW.** Dofetilide, a novel class III antiarrhythmic agent. *J Cardiovasc Pharmacol* 20, Suppl 2: S96–S105, 1992.
33. **Roche M, Renauleaud C, Ballet V, Douboyetzky M, Guillon JM.** The isolated rabbit heart and Purkinje fibers as models for identifying proarrhythmic liability. *J Pharmacol Toxicol Methods* In press.
34. **Roden DM.** Clinical practice Long-QT syndrome. *N Engl J Med* 358: 169–176, 2008.
35. **Rosenbaum MB, Acunzo RS.** Pseudo 2:1 atrioventricular block and T wave alternans in the long-QT syndromes. *J Am Coll Cardiol* 18: 1363–1366, 1991.
36. **Sakaguchi T, Shimizu W, Ito H, Noda T, Miyamoto Y, Nagaoka I, Oka Y, Ashihara T, Ito M, Tsuji K, Ohno S, Makiyama T, Kamakura S, Horie M.** Age- and genotype-specific triggers for lifethreatening arrhythmia in the genotyped long QT syndrome. *J Cardiovasc Electrophysiol* 19: 794–799, 2008.
37. **Salata JJ, Jurkiewicz NK, Jow B, Folander K, Guinasso PJ Jr, Raynor B, Swanson R, Fermini B.**  $I_{K1}$  of rabbit ventricle is composed of two currents: evidence for  $I_{Ks}$ . *Am J Physiol Heart Circ Physiol* 271: H2477–H2489, 1996.
38. **Taneja T, Windhagen Mahnert BW, Passman R, Goldberger J, Kadish A.** Effects of sex and age on electrocardiographic and cardiac electrophysiological properties in adults. *PACE* 24: 16–21, 2001.
39. **Varro A, Lathrop DA, Hester SB, Nanasi PP, Papp JG.** Ionic currents and action potentials in rabbit, rat, and guinea pig ventricular myocytes. *Basic Res Cardiol* 88: 93–102, 1993.
40. **Viswanathan PC, Rudy Y.** Pause induced early afterdepolarizations in the long QT syndrome: a simulation study. *Cardiovasc Res* 42: 530–542, 1999.
41. **Yan SH, Hu HS, Wang LX, Xing QC, Cheng WJ, Xue M.** Effects of angiotensin converting enzyme inhibition on cardiac innervation and ventricular arrhythmias after myocardial infarction. *Clin Invest Med* 31: E198–E205, 2008.
42. **Ziv O, Morales E, Song YK, Peng X, Odening KE, Buxton AE, Karma A, Koren G, Choi BR.** Origin of complex behaviour of spatially discordant alternans in transgenic rabbit model of type 2 long QT syndrome. *J Physiol* 587: 4661–4680, 2009.